Neural-Network-Based Multiobjective Optimizer for Dual-Band Circularly Polarized Antenna

Tarek Sallam [1,2], Ahmed M. Attiya [3], and Nada Abd El-Latif [3]

[1] Faculty of Electronic and Information Engineering
Huaiyin Institute of Technology, Huai'an 223002, Jiangsu, China

[2] Faculty of Engineering at Shoubra, Benha University, Cairo, Egypt
tarek.sallam@feng.bu.edu.eg

[3] Microwave Engineering Dept., Electronics Research Institute (ERI), Cairo, Egypt
attiya@eri.sci.eg

Abstract ─ A multiobjective optimization (MOO) technique for a dual-band circularly polarized antenna by using neural networks (NNs) is introduced in this paper. In particular, the optimum antenna dimensions are computed by modeling the problem as a multilayer feed-forward neural network (FFNN), which is two-stage trained with I/O pairs. The FFNN is chosen because of its characteristic of accurate approximation and good generalization. The data for FFNN training is obtained by using HFSS EM simulator by varying different geometrical parameters of the antenna. A two strip-loaded circular aperture antenna is utilized to demonstrate the optimization technique. The target dual bands are 835–865 MHz and 2.3–2.35 GHz.

Index Terms ─ Circularly polarized antenna, feed-forward neural networks, multiobjective optimization.

I. INTRODUCTION

Design of multiband single-fed circularly polarized antenna represents a complicated problem due to the requirements of obtaining matching properties combined with two equal orthogonal fields and phase shift of $\pm\pi/2$. For a single band circular polarized printed antenna, these conditions can be obtained by using symmetric shape structure like square or circular loaded by diagonal perturbations. By controlling the area of these perturbations compared to the total are of the printed antenna, it would be possible to generate two equal orthogonal modes along the printed antenna with the required phase shift [1, 2]. The design of these antenna configurations can be formulated analytically by using cavity model [1]. However, for the case of multiband single-fed circularly polarized antenna the problem becomes more complicated and cannot be directly represented in a simple cavity model. On the other hand, numerical simulation tools can be used to simulate different configurations to obtain the corresponding properties for these configurations but these numerical tools cannot be used directly to design for specific properties. Thus, it is required to combine machining learning tools with numerical simulation tools to introduce appropriate design for such complicated problems, which cannot be formulated in simple analytical models [3–6].

Solving multiobjective optimization problems (MOPs) with traditional optimization methods has been found to be difficult because these methods often require many complex computations and the common way in this case is to reduce the set of objectives into a single objective and handle it accordingly. On the other hand, artificial intelligence (AI) techniques have proved to be good alternatives so they are now widely utilized in solving MOPs. One of these techniques is Neural Networks (NNs). NNs [7] model biological neural systems. They have been applied to many real-world problems, as a data analysis tool to map nonlinear relationships between process inputs and outputs, especially in classification and pattern recognition. In addition, NNs have been applied to problems in optimization and linear programming. While NNs are developed from the field of AI and brain modeling, they can also be considered as function approximation tools, which learn the relationship between independent variables and dependent variables, much like regression or other more traditional approaches. The principal difference between NNs and statistical approaches is that NNs make no assumptions about the statistical distribution or properties of the data, and therefore NNs tend to be more useful in practical situations. NNs are also an inherently nonlinear approach giving them more accuracy when modeling complex data patterns. Moreover, when closed form solutions do not exist and trial-and-error methods are the only approaches to solving the problem (like the problem at hand). By

Submitted On: October 18, 2020
Accepted On: January 27, 2021

https://doi.org/10.47037/2020.ACES.J.360304

training an NN one can use it to predict solutions to the problem. These properties make NNs gaining a huge momentum in the field of RF and microwave modeling and design [8–14] mainly because of its generalization capability, nonlinear property, massive parallelism, adaptive learning capability, fast convergence rates, insensitivity to uncertainty, and VLSI implementations. Recently, NNs have been applied successfully to the field of RFID technology such as ranging [15], signal modeling [16], positioning [17], and sensing [18].

In [19], a dual-band circularly polarized RFID reader antenna is designed by using ramped convergence particle swarm optimization (RCPSO). This algorithm uses a multi-start approach to break down the optimization problem by considering only a subset of antenna dimensions at a time, hence overcoming the curse of dimensionality and premature convergence of classical PSO. However, this requires large execution time (about 10 hours for PSO and ~50 hours for RCPSO).

Motivated by the inherent advantages of NNs, this paper presents a feed-forward neural network (FFNN)-based multiobjective optimization (MOO) approach to design a dual-band circularly polarized antenna. NNs typically adopt two steps: training and recalling. The network is first trained with known input–output pattern pairs; although a large training pattern set may be required for network training, it can be implemented separately. After training, it can be used directly to replace the complex system dynamics. In this paper, the FFNN is trained on data generated by the HFSS simulator by varying the antenna dimensions. There are two stages of training/recalling.

II. FFNN ARCHITECTURE

A NN consists of a set of processing units, called nodes or neurons, connected by weighted arcs, where the weights represent the strength of connections. The nodes are organized into layers [7]. Nodes in the input layer called input nodes, accept input from the outside world and nodes in the output layer, called output nodes, generate output to the outside world. Nodes in the input layer are used to distribute inputs only and do not serve any processing or computational function. Nodes in layers between the input layer and the output layer called hidden nodes, and these layers are called hidden layers.

NNs can be of several kinds of architecture. They can contain one or more hidden layers of neurons and may have feedback connections or not. The NN architecture constructed for our purpose here is multilayer perceptron (MLP) network. The networks are of feed-forward ones in which the signals always propagate from the input to the output layer without any feedback connections. In addition to the MLP, there are other NN structures [7] used for antennas, for example, radial basis function (RBF) networks and self-organizing map (SOM) networks [20]. A list of applications of NNs for antennas and arrays is given in [21], along with the type of network structure used and the advantage/ disadvantage of application.

Figure 1 shows a FFNN of only two hidden layers. However, more hidden layers can be added. In each neuron (node), the scalar input z is transmitted through a connection that multiplies its strength by the scalar weight w, to form the product wz, again a scalar. This product may be added to a scalar bias b (much like a weight, except that it has a constant input of 1) to form the final argument of an activation function f. The most frequently used activation function is the sigmoid function.

An NN is trained to represent an unknown mapping by employing a training set (a collection of paired input and desired output vectors observed from the unknown mapping). The purpose in training a NN is to determine the values of the elements in the weight matrix **W** so that the NN can closely represent the unknown mapping. The training of a NN is accomplished by the following steps:

(1) Mapping input vectors from the training set by the current version of the NN to their computed output vectors.
(2) Comparing the computed output vectors with their respective desired output vectors in the training set, and then.
(3) Adjusting the values of the components of **W** so as to reduce any differences between the computed and desired output vectors.

After a number of training iterations, the connectivity weights and node biases of the NN converges to a set of values that minimizes the differences between the computed and desired output vectors, and the NN organizes itself internally to construct a model to represent the unknown mapping from the input space to the output space. Thus, any new input vector presented to an appropriately trained NN yields an output vector similar to the one that would have been given by the actual mapping.

In this kind of network, learning process is done by error back-propagation (BP) learning rule in which the weights between the connections are adjusted such that the mean square error (MSE) between the targets and the inputs of the training set is returned back through the layers of neural units and eventually minimized as the performance of the neural system is maximized.

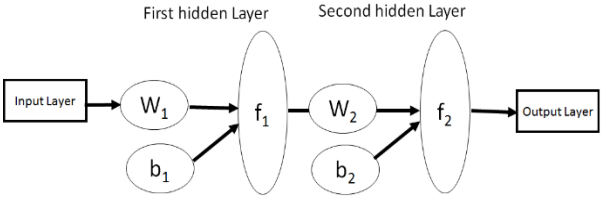

Fig. 1. The structure of FFNN

III. FFNN APPLICATION TO DESIGN A SINGLE-FED DUAL-BAND CIRCULARLY POLARIZED ANTENNA

As an example for utilizing FFNN in antenna design, the design of a single-fed multiband circularly polarized antenna is presented in this section. The proposed antenna is designed for multiband RFID reader system operating at two frequency bands; 835–865 MHz and 2.31–2.35 GHz, specifically. The required reflection coefficient of the antenna at these bands should be less than –10 dB and the corresponding axial ratio should be less than 3dB. The initial geometry of the proposed antenna is shown in Fig. 2. It is composed of a circular aperture in the ground plane of a grounded dielectric slab. The thickness of the substrate is $t = 1.6$ mm. The substrate is FR4 material with a dielectric constant $\varepsilon_r = 4.6$ and loss tangent $\tan\delta = 0.02$. The effective dielectric constant on the circular aperture can be approximated as $\varepsilon_{re} \approx (\varepsilon_r + 1)/2$. For this effective dielectric constant, the radius of a circular aperture which would be resonant at the center frequency of the lower band; 850 MHz, can be obtained approximately as $R = 46$ mm. This approximation is based on the assumption that the field distribution in this case is the dominant TE_{11} mode field distribution along a circular aperture of radius R [24]. This aperture is printed on a square substrate of length $L = 108$ mm. Two arbitrary conducting strips are printed on the other side of the dielectric slab. One of these two conducting strips are used as a feeding strip to the circular aperture while the other strip is a parasitic one which is used to introduce the required perturbation to obtain circular polarization.

It should be noted that, the position of the feeding strip is chosen to be near the center of the aperture to increase the coupling effect between the TE_{11} mode in the circular aperture and the feeding polygon. On the other hand, the parasitic strip is located near the edge of the circular aperture and nearly parallel to the feeding strip to introduce a small coupling with the excited TE_{11} mode in the circular aperture. This small coupling represents the required perturbation to introduce the required circular polarization. Each strip is a polygon composed of four corners. For each polygon, the *xy* coordinates of three corners are variable while the fourth corner is fixed constant. In addition, the two corners of the polygon at the feeding edge of the substrate have a constant value of *x* which corresponds to the *x* position of this edge. Thus, the total number of variables in this case for the two strips is ten variables. These ten variables can be used introduce infinite configurations for these two strips while keeping their starting positions at the feeding edge. The limits of these variables are chosen such that the two strips would lie within the dimensions of the substrate as well as the two strips should not be intersecting. Assuming that the center of the circular aperture is located at $x = 0$ and $y = 0$, the starting *xy* coordinates of the two strips would be as presented in Table 1.

Table 1: Initial values of the corners of the two strips

Corner No.	Strip#1 (Feeding Strip)		Strip#2 (Parasitic Strip)	
	x (mm)	*y* (mm)	*x* (mm)	*y* (mm)
1	54 (Fixed)	–18 (Fixed)	54 (Fixed)	49 (Fixed)
2	–32	–18	–35	42
3	8	–11	–30	40
4	54 (Fixed)	–10	54 (Fixed)	46

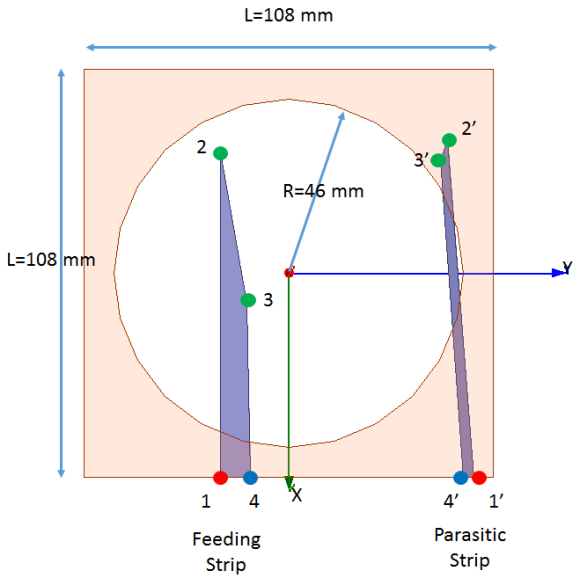

Fig. 2. Initial geometry of the proposed circular aperture antenna with its feeding and parasitic strips. The center of the antenna is located at the origin. The corners of the feeding strip and the parasitic strip are numbered from 1 to 4. The positions of the first corner for both the feeding and the parasitic strips are fixed and marked with red marker. The *x*-positions of the fourth corner for both the feeding and the parasitic strips are fixed while the *y*-positions are variable. These points are marked with blue marker. The second and the third corners for both strips are variable for both *x* and *y*. The points are marked in green. The initial values for these corners are presented in Table 1.

These variable parameters are presented as a variable vector **D** of ten elements which are $[x_2, y_2, x_3, y_3, y_4, x_{2\prime}, y_{2\prime}, x_{3\prime}, y_{3\prime}, y_{4\prime}]$ The initial values of these variable parameters according to Table 1 are: $\mathbf{D} = [-32, -18, 8, -11, -10, -35, 42, -30, 40, 46]^T$.

Figure 3 shows the results of this initial design

obtained by using HFSS. It can be noted that the resonance of this initial design is nearly around 750 MHz while the reflection coefficient of the antenna 2.35 GHz is only about –3dB. On the other hand, the axial ratio is greater than 8 dB in the two bands.

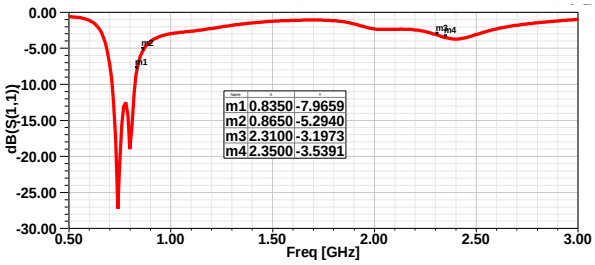

(a)

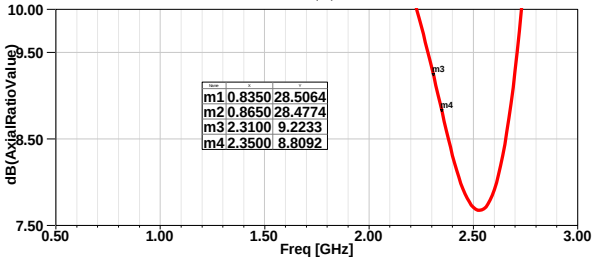

(b)

Fig. 3. Simulation results for the proposed antenna with initial parameters of the two strips: (a) reflection coefficient of the antenna, and (b) axial ratio of the radiation pattern in the broadside direction.

IV. THE FFNN-BASED MOO MODEL

One of the applications of NNs is *optimization*, where the aim is to find the optimal values of parameters in an optimization problem [22]. In this paper, The FFNN-based MOO model is used in a reverse way (inverse modeling) in which design variables are derived from objectives [23], where the input layer of the FFNN represents the objectives and the output layer represents the parameters to be optimized. Figure 4 shows the general FFNN-based model for solving MOPs.

Figure 5 shows the FFNN-based MOO model for the design of RFID reader antenna. Here, we have two objectives, the reflection coefficient ($|S_{11}|$) and axial ratio (AR). Thus, the input objective vector is [$|\mathbf{S_{11}}|$ | **AR**], where the vector $|\mathbf{S_{11}}|$ represents the linear-scale (to be in the range [0,1] suitable for NN training) values of $|S_{11}|$ in the target two bands, while the vector **AR** contains the linear-scale values of *AR* in both bands (normalized by its norm to unify the input parameter space). The target two bands are 835–865 MHz and 2.31–2.35 GHz. The frequency step is taken as 0.01 GHz, so we have 9 values for both $|\mathbf{S_{11}}|$ and **AR** (4 in lower band and 5 in the higher band). Therefore, the dimension of the input vector is 18 with the input layer of the FFNN having 18 neurons.

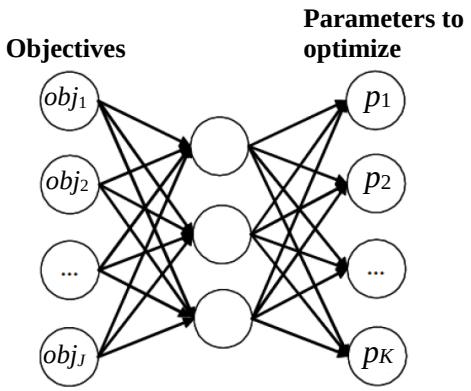

Fig. 4. The general FFNN-based MOO model.

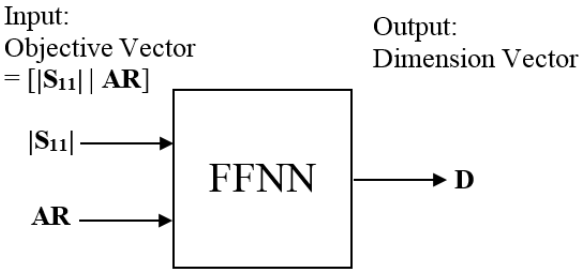

Fig. 5. The FFNN-based MOO model for the design of the proposed antenna.

To design a symmetric FFNN it is preferred to reduce the number of variables dimensions of the antenna to be nine instead of ten. This can be obtained by fixing any one of these variables. Thus, in the present analysis, the *y* position of the third corner of the first strip is fixed at –11 mm. It should be noted that this is an arbitrary choice and other choices are also possible. Thus, the remaining variables to be optimized would be nine variables. The output from FFNN in this case is the vector $\mathbf{D}'$ of the nine antenna variables. It should be noted that, each variable in the vector $\mathbf{D}'$ is normalized by using its minimum and maximum values to be in the range [0,1] for FFNN training. In this way, the size of the output layer of the FFNN is 9 neurons. The initial absolute value of the vector **D** in this case is $|\mathbf{D}| = [32,18,8,10,35,42,30,40,46]^T$.

Thus, the size of any training pattern will be 27, 18 inputs and 9 outputs. After many experimental simulation trials, it is found that three hidden layers with 10, 15, and 20 neurons, provide the best accuracy. Based on the above analysis, the final FFNN model is 18:10:15:20:9. The training patterns are extracted from the HFSS simulator by varying the nine dimensions of antenna along two stages of training/recalling. In either stage, 80% of total training patterns is randomly chosen for training and remaining 20% for validation.

The FFNN is trained using BP algorithm, which is implemented in C++. In the recalling, the trained FFNN is given the desired input vector, which contains the desired values of $|S_{11}|$ and *AR* over dual-band, to output the corresponding antenna dimensions. The recalling is also implemented by C++.

V. RESULTS AND DISCUSSIONS

A. Stage1 training/recalling

In the first stage of FFNN training/recalling, only one dimension is varied between its minimum and maximum values with a certain step, while all other dimensions are kept constant at their default values. The vectors of minimum, maximum absolute values are $|\mathbf{D}_{min,stg1}| = [27,13,3,5,30,37,25,35,41]^T$ and $|\mathbf{D}_{max,stg1}| = [37,23,13,10,40,47,35,45,51]^T$, respectively, with ten steps from the minimum to the maximum value for each variable. In this way, we have a total of 99 training patterns. The final MSE is 0.000891 after 500,000 iterations. The total training time is about 15 min. After the training, the FFNN is recalled and the output dimensions were $|\mathbf{D}_{stg1}| = [29.58,31.53, 7.7,10,38,24.87, 33.43,24.87,48.13]^T$. Then, these output dimensions are simulated in HFSS and the simulations results are shown in Fig. 6. Compared to the antenna with default dimensions (before optimization) shown in Fig. 3, it can be noted that the performances of $|S_{11}|$ and *AR* have been improved in both bands after the first stage of optimization. However, $|S_{11}|$ has a better performance in lower band than in higher band, and vice versa for *AR*.

B. Stage2 training/recalling

In the second stage of FFNN training/recalling, the training data is generated by HFSS by simulating 100 different sets of dimensions (100 training patterns). In order to exploit the results of stage1, the dimensions in this stage are randomly generated *around* the output dimensions from stage1 $\mathbf{D}_{stg1}$ using normal distribution keeping them as *means* and using a constant variance of 5 for all dimensions. In this case, The vectors of min and max dimensions are $\mathbf{D}_{min,stg2} = \mathbf{D}_{stg1} - \mathbf{5}$ and $\mathbf{D}_{max,stg2} = \mathbf{D}_{stg1} + \mathbf{5}$, where **5** is a vector with all elements are equal 5. The final MSE is 0.000015 after 500,000 iterations. The total training time is about 20 min. After the training, the FFNN is recalled and the output dimensions were $\mathbf{D}_{stg2} = \mathbf{D}_{final}$ = [26.26, 37, 12.89, 14.92, 33, 23.41, 37.55, 18.41, 48.89]. The corresponding final values of the corners of the two strips are presented in Table 2. The final configuration is simulated by using HFSS and the simulations results are shown in Fig. 7.

Compared to stage1 in Fig. 6, it can be noted from Fig. 7 that $|S_{11}|$ and *AR* have overall better results in target bands with much improvement in UHF band for both of them. $|S_{11}|$ has still better performance in UHF band than in SHF, but for AR, the performances in both bands now become almost equal with a deeper notch in UHF band. In addition, it can be seen from Fig. 7 that after the second stage of optimization, $|S_{11}|$ and *AR* are beneath –10 dB and 3 dB, respectively, in both bands of interest, allowing the final optimized antenna to be considered as a universal RFID reader antenna.

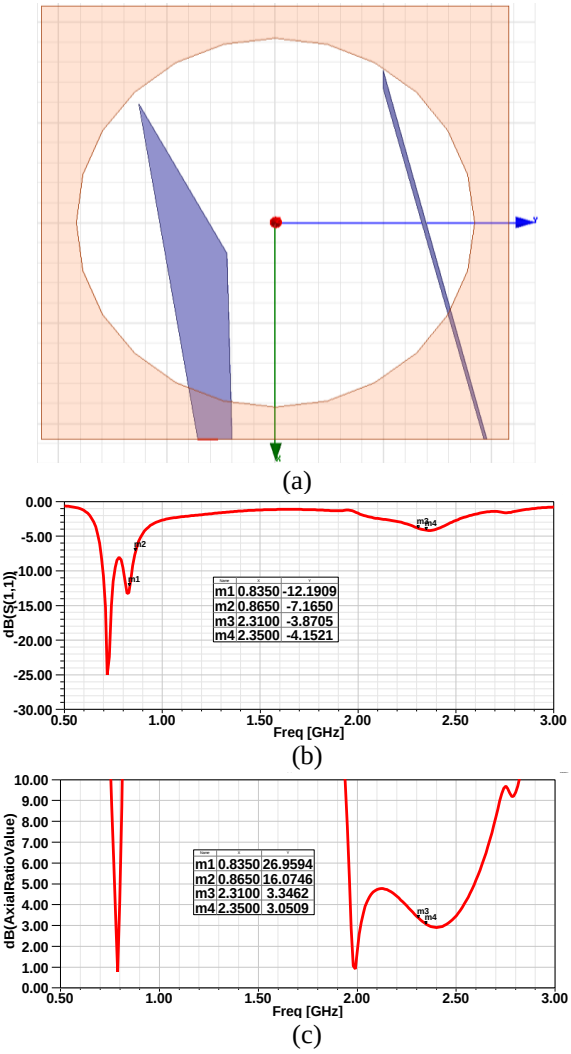

Fig. 6. The output from stage1 training/recalling: (a) geometry of the antenna, (b) reflection coefficient of the antenna, and (c) axial ratio.

Table 2: Final values of the corners of the two strips

Corner No.	Strip#1 (Feeding Strip)		Strip#2 (Parasitic Strip)	
	x (mm)	*y* (mm)	*x* (mm)	*y* (mm)
1	54 (Fixed)	–18 (Fixed)	54 (Fixed)	49 (Fixed)
2	–26.26	–37	–33	23.41
3	12.89	–11 (Fixed)	–37.55	18.41
4	54 (Fixed)	–14.92	54 (Fixed)	48.89

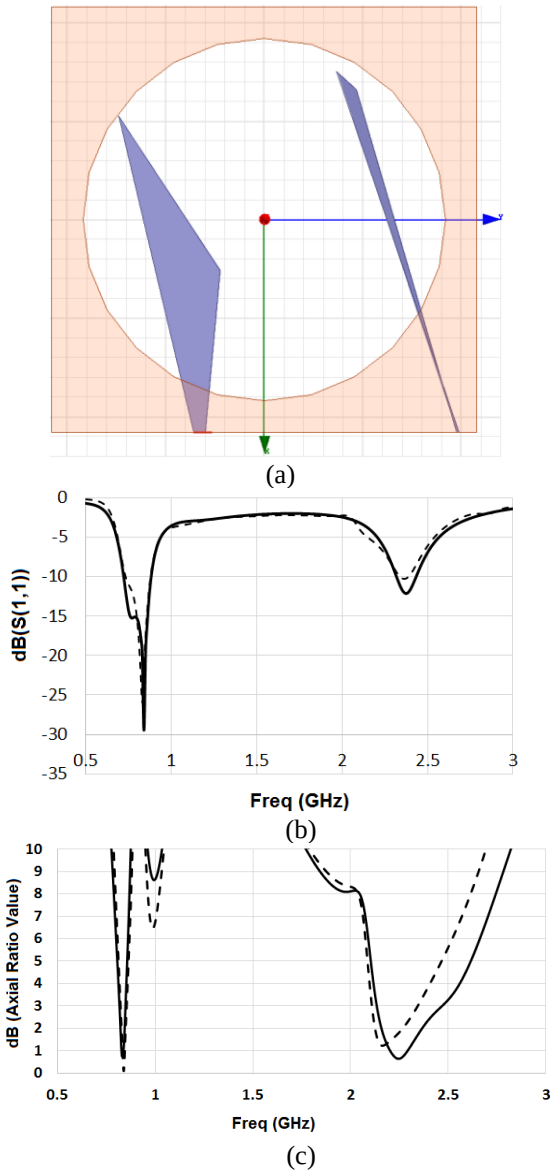

Fig. 7. The output (final) from stage2 training/recalling: (a) geometry of the antenna, (b) reflection coefficient of the antenna, and (c) axial ratio. Solid line by using HFSS and dashed line by using CST.

To verify the obtained result, the same structure with its final dimensions is simulated by using CST. Figure 7 shows a comparison between the results of the HFSS (solid line) and CST (dashed line) simulations. Good agreements between the results of the two simulation techniques are obtained for both the reflection coefficient and the axial ratio of the designed antenna structure with its final dimensions.

VI. CONCLUSION

A dual band circularly polarized antenna is presented in this paper. The proposed antenna is composed of a circular aperture on a grounded dielectric slab. This circular aperture is fed by a feeding strip and perturbed by another parasitic strip to introduce circular polarization. The shape and dimensions of these two strips are optimized by using a NN-based MOO model. Each strip has four corners. Each corner has two variables; x and y positions. Thus, the total number of variables is sixteen. To make the starting point of each strip fixed at the edge of the substrate, the starting corners for the two strips are fixed. Thus, four variable are assumed to be constant. In addition, the last corner at each strip is assumed to be located on the edge of the substrate. Thus, the x values for the last corners on the two strips are also constant. Thus, the remaining number of variables is ten. The notable benefits of the proposed NN model are simplicity and accurate determination of the characteristic parameters of the antenna. The NN model is accurate enough to yield the parameters of the antenna thus eliminating the long time consuming process of determination various design parameters using costly software packages. A distinct advantage of neural model computation is that after proper training, a NN completely bypasses the repeated use of complex iterative processes for new cases presented to it. The total training time was just about 35 min. The optimized design is compact and exhibits less than –10 dB $|S_{11}|$ and 3 dB *AR* in both bands making it practically ideal dual-band circularly polarized RFID reader antenna.

REFERENCES

[1] J. R. James and P. S. Hall, *Handbook of Microstrip Antennas*. IET, 1989.

[2] S. S. Gao, Q. Luo, and F. Zhu, *Circularly Polarized Antennas*. John Wiley & Sons, 2013.

[3] C. Wang, J. Li, A. Zhang, W. T. Joines, and Q. H. Liu, "Dual-band capacitively loaded annular-ring slot antenna for dual-sense circular polarization," *Journal of Electromagnetic Waves and Applications*, vol. 31, no. 9, pp. 867-878, 2017.

[4] K. M. Mak, H. W. Lai, K. M. Luk, and C. H. Chan, "Circularly polarized patch antenna for future 5G mobile phones," *IEEE Access*, vol. 2, pp. 1521-1529, 2014.

[5] H. Yang, Y. Fan, X. Liu, and M. M. Tentzeris, "Single-fed dual-band circularly polarized patch antenna with wide 3-dB axial ratio beamwidth for CNSS applications," *2019 IEEE MTT-S International Wireless Symposium (IWS)*, pp. 1-3, 2019.

[6] K.-L. Lau, K.-M. Luk, and K.-F. Lee, "Design of a circularly-polarized vertical patch antenna," *IEEE Transactions on Antennas and Propagation*, vol. 54, no. 4, pp. 1332-1335, Apr. 2006.

[7] S. Haykin, *Neural Network: A Comprehensive Foundation*. Upper Saddle River, NJ, USA: Prentice-Hall, 1999.

[8] Q. J. Zhang and K. C. Gupta, *Neural Networks for RF and Microwave Design*. Boston, MA: Artech House, 2000.

[9] T. Sallam, A. B. Abdel-Rahman, M. Alghoniemy, and Z. Kawasaki, "A novel approach to the recovery of aperture distribution of phased arrays with single RF channel using neural networks," *2014 Asia-Pacific Microwave Conference*, Sendai, Japan, pp. 879-881, 2014.

[10] T. Sallam, A. B. Abdel-Rahman, M. Alghoniemy, Z. Kawasaki, and T. Ushio, "A Neural-network-based beamformer for phased array weather radar," *IEEE Transactions on Geoscience and Remote Sensing*, vol. 54, no. 9, pp. 5095-5104, Sept. 2016.

[11] L. Liu, Z. Guan, G. Shen, P. Zhao, and G. Wang, "Parameters extraction for equivalent circuit model based on artificial intelligence," *2019 IEEE International Conference on Computational Electromagnetics (ICCEM)*, Shanghai, China, pp. 1-3, 2019.

[12] L. Yuan, X. Yang, C. Wang, and B. Wang, "Multibranch artificial neural network modeling for inverse estimation of antenna array directivity," *IEEE Transactions on Antennas and Propagation*, vol. 68, no. 6, pp. 4417-4427, June 2020.

[13] S. Rani and J. S. Sivia, "Design and development of virtual instrument for fault diagnosis in fractal antenna array," *Int. J. RF Microw. Comput. Aided Eng.*, vol. 30, no. 1, 2020.

[14] S. Dutta, B. Basu, and F. A. Talukdar, "Cascaded neural network based small array synthesis with robustness to noise," *Int. J. RF Microw. Comput. Aided Eng.*, vol. 31, no. 1, 2021.

[15] M. Agatonovic, E. Di Giampaolo, P. Tognolatti, and B. Milovanovic, "Artificial neural networks for ranging of passive UHF RFID tags," *2013 11th International Conference on Telecommunications in Modern Satellite, Cable and Broadcasting Services (TELSIKS)*, Nis, pp. 505-508, 2013.

[16] Z. Chen and C. Wang, "Modeling RFID signal distribution based on neural network combined with continuous ant colony optimization," *Neurocomputing*, vol. 123, pp. 354-361, 2014.

[17] J. Wang, W. Wei, W. Wang, and R. Li, "RFID hybrid positioning method of phased array antenna based on neural network," *IEEE Access*, vol. 6, pp. 74953-74960, 2018.

[18] S. Jeong, M. M. Tentzeris, and S. Kim, "Machine learning approach for wirelessly powered RFID-based backscattering sensor system," *IEEE Journal of Radio Frequency Identification*, vol. 4, no. 3, pp. 186-194, Sept. 2020.

[19] S. Kibria, M. T. Islam, and B. Yatim, "New compact dual-band circularly polarized universal RFID reader antenna using ramped convergence particle swarm optimization," *IEEE Transactions on Antennas and Propagation*, vol. 62, no. 5, pp. 2795-2801, May 2014.

[20] C. G. Christodoulou and M. Georgiopoulos, *Applications of Neural Networks in Electromagnetics*. Artech House, Boston, 2001.

[21] C. G. Christodoulou and A. Patnaik, "Neural networks for antennas," *In Modern Antenna Handbook*, C. A. Balanis (Ed.), pp. 1625-1657, 2008.

[22] A. P. Engelbrecht, *Computational Intelligence: An Introduction*. John Wiley & Sons, 2007.

[23] K. Kobayashi, M. Miki, and T. Hiroyasu, "Mechanism of multi-objective genetic algorithm for maintaining the solution diversity using neural network," *In Lecture Notes in Computer Science*, vol. 4403, pp. 216-226, 2007.

[24] C. A. Balanis, *Antenna Theory: Analysis and Design*. 3rd Ed., John Wiley & Sons. Inc, 2005.